Generation of high quality ion beams through the stable radiation pressure acceleration of the near critical density target*

Xue-Ren Hong(洪学仁)[1], Wei-Jun Zhou(周伟军)[1,†], Bai-Song Xie(谢柏松)[2], Yang Yang(杨阳)[1], Li Wang(王莉)[1], Jian-Min Tian(田建民)[1], Rong-An Tang(唐荣安)[1], and Wen-Shan Duan(段文山)[1]

[1] *Key Laboratory of Atomic and Molecular Physics & Functional Materials of Gansu Province, College of Physics and Electronic Engineering, Northwest Normal University, Lanzhou* 730070, *China*

[2] *College of Nuclear Science and Technology, Beijing Normal University, Beijing* 100875, *China*

(Received 7 January 2017; revised manuscript received 9 March 2017; published online 20 April 2017)

In order to generate high quality ion beams through the stable radiation pressure acceleration (RPA) of the near critical density (NCD) target, we propose a new type of target where an ultra-thin high density (HD) layer is attached to the front surface of an NCD target, which has a preferable self-supporting property in the RPA experiments than the ultra-thin foil target. It is found that in one-dimensional particle-in-cell (PIC) simulation, by the block of the HD layer in the new target, there emerges the hole-boring process rather than propagation in the NCD layer when the intense laser pulse impinges on this target. As a result, a typical RPA structure that the compressed electron layer overlaps the ion layer as a whole is formed and a high quality ion beam is obtained, e.g., a circularly polarized laser pulse with normalized amplitude $a_0 = 120$ impinges on this new target and a 1.2 GeV monoenergetic ion beam is generated through the RPA of the NCD layer. Similar results are also found in the two-dimensional PIC simulation.

Keywords: laser plasma interaction, radiation pressure acceleration, near critical density target

PACS: 52.38.Kd, 52.65.Rr, 41.75.Jv **DOI:** 10.1088/1674-1056/26/6/065203

1. Introduction

High quality ion beams acceleration through the laser-plasma interaction has been widely studied for the past few decades because of its many significant applications, such as low-cost tabletop accelerators,[1] hadron therapy of oncological diseases,[2] and inertial confinement fusion.[3–5] A number of acceleration mechanisms have been proposed, for instance, electrostatic shock acceleration,[6–9] target normal sheath acceleration,[10–12] magnetic vortex acceleration,[13–16] and radiation pressure acceleration (RPA),[17–35] etc. Among all these mechanisms, the RPA that by using the circularly polarized laser, in which the generation of the hot electron is effectively suppressed and the steady radiation pressure is dominated,[17,22,33,36] is regarded as the highly promising scheme due to the high energy conversion efficiency and the production of the high-quality fast ions.[17,23,34] In the RPA, the acceleration process contains two stages, the hole-boring (HB) stage and the light-sail (LS) stage. In the HB stage, the light pressure of the laser pulse compresses and deforms the front surface of the target, which allows the laser pulse to penetrate deeply into the target.[29,33] In the LS stage, the compressed electron layer overlaps the ion layer and they form a quasi-electric-neutral plasma mirror, which detaches from the target and is boosted as a whole by the light pressure of the laser pulse.[31,33]

In the RPA experiment, the ultra-thin foil target is conventionally used due to their high density,[33] which can block the intense laser pulse and generate a strong charge separation field. Therefore, the ions in the target could have enough time to respond to the field and catch up with the fast moving electron layer. Eventually, the RPA structure that the electron layer overlaps the ion layer as a whole can be formed and the ions in this structure are able to be accelerated to a high energy in the LS stage.[23] However, the thickness range of the ultra-thin target is usually from tens of nanometres to micrometre,[31] which leads to a terrible self-supporting property in reality. Hence, such a vulnerable target should increase the difficulty of the experiment operation. An ideal solution is to reduce the density and increase the thickness of the target. Therefore, the near-critical density (NCD) target, whose density is usually from $0.1n_c$ to $10n_c$, is a feasible substitution to the ultra-thin foil target, where $n_c = m_e\omega^2/4\pi e^2$ is the critical density, m_e and $-e$ are the electron rest mass and charge, and ω is the frequency of the laser, respectively.

Recently, the NCD target has drawn wide interests and a series of investigations about the interactions of the laser pulse with the NCD target have been presented.[16,36–40] For example: making the NCD layer as a laser shaping instrument to obtain a steep-front laser pulse,[36] realizing the electron acceler-

*Project supported by the National Natural Science Foundation of China (Grant Nos. 11365020, 11475026, 11565022, and 11547304), the Science and Technology Program of Gansu Province of China (Grant No. 1606RJZA090), the Fundamental Research Funds for the Higher Education Institutions of Gansu Province of China (2012), the Foundation of Northwest Normal University (Grant Nos. NWNU-LKQN-14-9 and NWNU-LKQN-16-3), and partially supported by the Fundamental Research Funds for the Central Universities of China.

†Corresponding author. E-mail: zwj_nwnu@163.com

© 2017 Chinese Physical Society and IOP Publishing Ltd

ation by using two consecutive laser pulses interacting with an NCD target[37] or through the direct laser acceleration[38] and the relativistic resonant phase locking[39] in the NCD region, and generating the high-quality ion beams by the laser wake field acceleration[40] or the magnetic vortex acceleration[16] in the NCD region. However, there is little detailed research about the RPA of the NCD target until now. In this paper, we investigate the monoenergetic ion beam acceleration through the RPA of the NCD target by proposing a new type of target that a high density (HD) layer is attached to the front surface of the NCD target.

The organization of this paper is as follows. In Section 2, we investigate the difficulty of realizing the RPA of the NCD target through an intense laser pulse that radiates on an NCD target directly. Therefore, we propose a new target structure scheme that an ultra-thin HD layer is attached to the front surface of the NCD layer and hope to realize the RPA of the NCD layer. In Section 3, one-dimensional (1D) and two-dimensional (2D) particle-in-cell (PIC) simulations by using the relativistic electromagnetic PIC code VORPAL[41] are proposed to verify this new scheme. In Section 4, the conclusion about this new scheme and the potential applications are presented.

2. Model

In the RPA, the energy of the accelerated ions in different RPA stages is related to the intensity of the laser pulse with different scales. In the HB stage, the ion energy is[28]

$$\varepsilon_{\mathrm{i}} = m_{\mathrm{i}}c^2 \frac{2\Xi}{1+2\Xi}. \tag{1}$$

In the LS stage, the ion energy is[17]

$$\varepsilon_{\mathrm{i}} \approx \left(1 - \frac{1}{4\gamma^2}\right)\varepsilon_L, \tag{2}$$

where $\Xi = I/m_{\mathrm{i}}n_{\mathrm{i}}c^3$ is the dimensionless laser pistoning parameter, I is the intensity of the laser, m_{i} and n_{i} are the mass and density of the ion respectively, c is the vacuum light speed, $\gamma = (1 - v^2/c^2)^{-1/2}$ is the Lorentz factor of the plasma mirror, v is the speed of the plasma mirror in the laboratory reference frame, $\varepsilon_L \propto IL$ is the energy of the laser pulse, and L is the pulse length. From Eqs. (1) and (2), it can be found that, in order to generate the higher energy ion beams through the RPA, the most direct way is to increase the intensity of the laser pulse. However, in the high laser intensity region, it is hard to realize the RPA of the NCD target directly due to the following two reasons. Firstly, in the high laser intensity region, there is a relativistic correction of the critical density as follows:[42]

$$n_{\mathrm{c}}' = \gamma n_{\mathrm{c}}, \tag{3}$$

where $\gamma = (1 + a_0{}^2)^{1/2}$ is the relativistic factor, and the laser normalized amplitude $a_0 = eE_0/m_{\mathrm{e}}\omega c$, E_0 is the amplitude of the laser electric field. It can be found from Eq. (3) that, when an ultra-intense laser with the wavelength $\lambda = 1$ μm and the normalized laser amplitude $a_0 = 120$ radiates on an NCD target, of which the initial electron density $n_{\mathrm{e}} = 2n_{\mathrm{c}}$, the relativistic critical density $n_{\mathrm{c}}' \sim 120n_{\mathrm{c}}$. In consequence, the laser pulse will propagate in the NCD target without restriction. Secondly, the ion response time is[43]

$$\tau_{\mathrm{i}} = \sqrt{\frac{m_{\mathrm{i}}}{4\pi Ze^2 n_{\mathrm{i}}}}, \tag{4}$$

where Z is the effective nuclear charge number of the ion. From Eq. (4), it can be found that, due to the lower ion density of the NCD target, the ion response time of the NCD target is much longer than that of the ultra-thin solid target. As a result, when an intense laser pulse impinges on an NCD target directly, the electrons are pushed forward so quickly while the ions have almost not responded to the field yet. Eventually, extremely strong light pressure acts on the compressed electron layer and expels them from the target. With the combined effects of the inner Coulomb repulsion with the acceleration field, the energy spread of the accelerated ions become broad and the majority of the ions are still in the low energy region, which is also proved from the following simulations in Section 3. Therefore, it is hard to generate a high quality ion beam through an intense laser pulse impinging on a NCD target directly.

For realizing the RPA of the NCD target, a new type of target is proposed and the schematic of the new target is shown in Fig. 1. By attaching an ultra-thin HD layer in the front of the NCD layer, the relativistic self-induced transparency of the NCD layer would be settled. This HD layer can lead to a dense surface density, which can effectively reduce the laser penetrating velocity in the NCD layer. Besides, the separation of charged particles in the HD layer can generate enough high charge separation field at the beginning of the interaction, which gives rise to a sufficiently strong acceleration field for the ions in the NCD layer. In consequence, when the intense laser pulse enters the NCD layer, the ions in the NCD layer may catch up with the fast-moving electron layer in such a strong accelerating field. Therefore, there should emerge the HB process rather than the propagation in the NCD layer. After the HB stage, the typical RPA structure would be formed and a high quality ion beam could be generated through the RPA of the NCD layer.

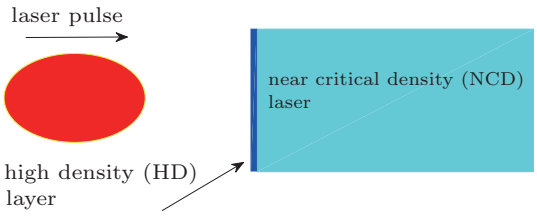


Fig. 1. (color online) Schematic diagram for the RPA of the HD-NCD target.

Since the proton has the highest charge-to-mass ratio among all ions, which means the highest acceleration efficiency in the RPA,[33] we choose the pure hydrogen as the target material of the NCD layer. In addition, two other difficulties of the RPA are the loss of the electrons and the development of instability in the acceleration, which would lead to the transparency of the electron layer and broaden the energy spread of the accelerated ions.[32] In order to realize a more efficient stable RPA of the proton, a lower charge-to-mass ratio target material should be used in the HD layer, which works as a "buffer" of instability[30] and also can supply the abundant electrons to the front electron layer to maintain the quasi-electric-neutral RPA structure, which is known as the leaky light-sail regime.[31] The difference is, in previous researches about the mixed multi-species foil target,[30–32] there is a time lag for the initial mixed ions layer evolved into the layered ions layers, i.e., light ion layer in the front and heavy ion layer in the back, in the acceleration process. Therefore, it would take a while for the heavy ions to come into play. However, in our scheme, we have set that the heavy and light ions are separated initially, and placed in the HD layer and the NCD layer respectively. There are two reasons for this specific structure of the new target. On the one hand, there is no time lag for the separation of the heavy and light ion layers due to our target structure, and the stable RPA ion structure, layered ions layers, could be formed earlier than the common mixed multi-species foil target. On the other hand, the Coulomb repulsion from the heavy ions to the light ions, which has a contribution to the acceleration of the light ions,[25,32] would start to work while the laser penetrates the HD layer. The light ions under the ultra strong accelerating field can be accelerated very efficiently at the beginning of the interaction, just like being shot by a "slingshot". Therefore, we use the carbon ion in the HD layer. By this new scheme, it is expected that the stable RPA of the NCD layer can be realized and a high energy proton beam with low energy spread can be generated.

3. Simulation and results

3.1. One-dimensional case

In this part, the 1D PIC simulations are performed to verify our new scheme. For the new scheme (HD-NCD target), the length of the simulation box is 111 μm, and the grid resolution is 0.01 μm. A circularly polarized laser pulse with a Gaussian envelope $a = a_0 \exp\left[-(1/2)(t-t_0)^2/T_0^2\right]$ in the longitudinal (x) normally radiates on the target from the left. The normalized laser amplitude $a_0 = eE_0/m_e\omega c = 120$, corresponding to the laser intensity $I = 3.95 \times 10^{22}$ W/cm^2 with the laser wavelength $\lambda = 1$ μm. The laser period $T_L = 3.3$ fs, and $t_0 = T_0 = 10T_L$. The HD layer which consists of the fully ionized carbon ions and electrons is located in the region 20.0 μm $< x <$ 20.1 μm with the initial electron density $n_{e1} = 360n_c$. Here, the normalized amplitude of the laser pulse, the thickness and the initial electron density of the HD layer satisfy the optimum target thickness relation[24]

$$\frac{l_{opt}}{\lambda} \sim \frac{1}{\pi}\frac{n_c}{n_{e1}}a_0, \tag{5}$$

where l_{opt} is the optimum target thickness. At $t = 0$, the front edge of the laser pulse reaches the front surface of the HD layer. The NCD layer which consists of the protons and electrons is located in the region 20.1 μm $< x <$ 24.0 μm, and the initial electron density $n_{e2} = 2n_c$. On the other hand, we also performed a comparative simulation (NCD target). In the comparative simulation, there is no HD layer in the target, i.e., a single NCD layer is located in the region 20.1 μm $< x <$ 24.0 μm, and the other parameters are the same as those of the HD-NCD target.

Firstly, figure 2 shows the snapshots of the spatial density distributions of the electron and the proton and the longitudinal electric field at $t = 1T_L$, $t = 4T_L$, $t = 9T_L$, and $t = 26T_L$, respectively. Figures 2(a1)–2(a4) represent the results of the NCD target, and figures 2(b1)–2(b4) represent the results of the HD-NCD target. For the NCD target, at the beginning of the interaction, as seen in Fig. 2(a1), the electron layer is pushed forward so quickly by the light pressure of the intense laser pulse, and the protons in a weak charge separation field cannot catch this fast moving electron layer and remain at rest. Until the laser pulse penetrates through the NCD target, as shown in Fig. 2(a2), the electron layer is expelled from the target and the protons are nearly still in their initial positions. After that, the protons are continually dispersed due to the Coulomb explosion[25] and the forward acceleration field, as seen in Figs. 2(a3) and 2(a4). Therefore, it is unable to form an RPA structure in the NCD target. However, in the HD-NCD target, as seen in Fig. 2(b1), by the block of the attached ultrathin HD layer, the laser penetrating velocity is effectively reduced and the laser pulse is just boring the HD layer at $t = 1T_L$. Meanwhile, a strong charge separation field is generated by the charged particles' separation of the HD layer. It can be seen that in Fig. 2(b2), a clear density peak of the proton emerges behind the electron layer. As the process of the HB, the protons are gradually caught in the RPA field and catch up with the electron layer. Finally, at the end of the HB stage, the proton layer is tied together with the compressed electron layer by the charge separation field, as presented in Fig. 2(b3). In the LS stage, as shown in Fig. 2(b4), the electron layer overlaps the proton layer as a whole, and forms a quasi-electric-neutral plasma mirror, which is boosted by the laser pulse and gets further acceleration.

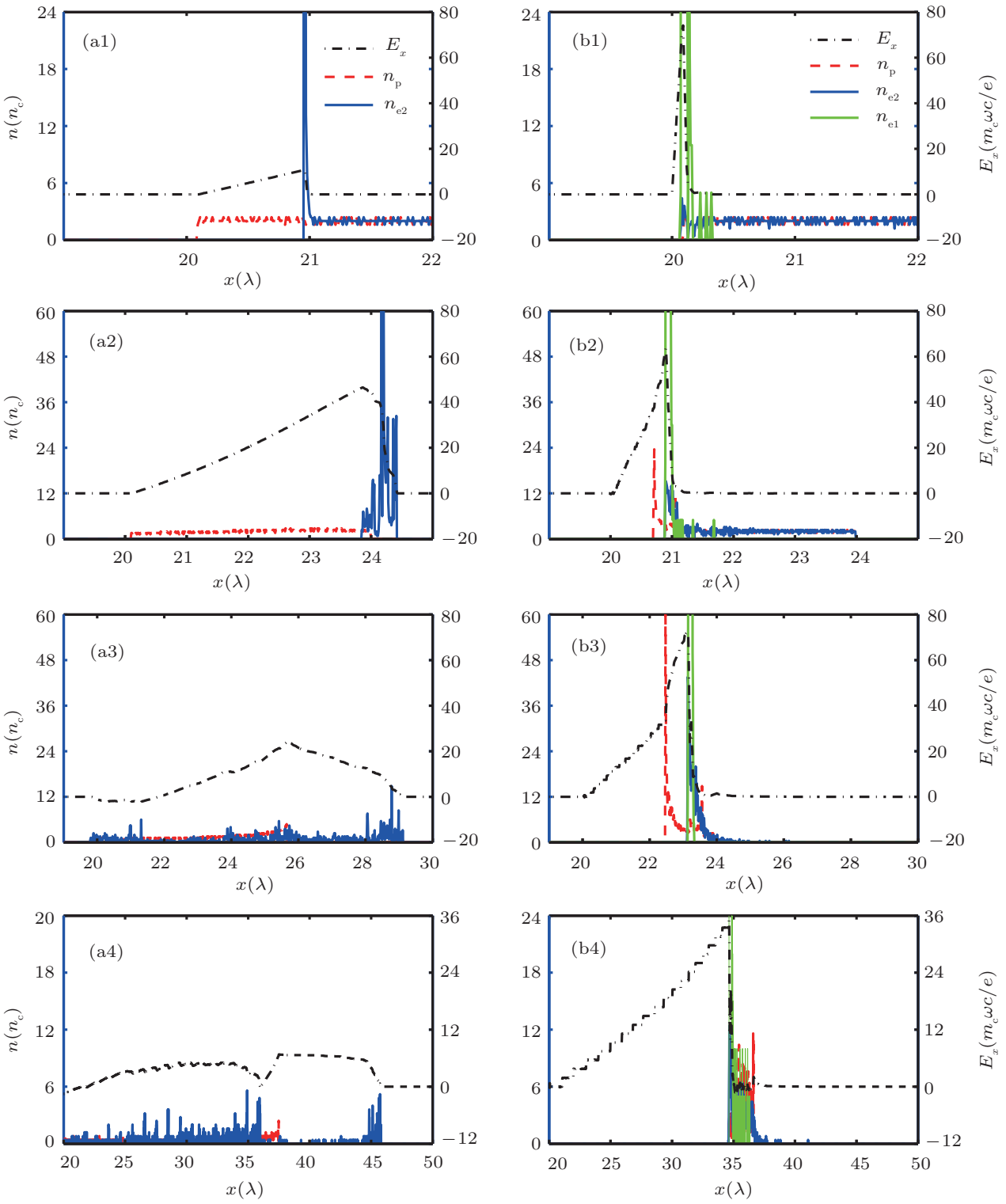


Fig. 2. (color online) The normalized density distributions of the electron and the proton in the 1D simulations. The left column is the result of the NCD target and the right column is of the HD-NCD target. Here, the green solid line denotes the electron density n_{e1} of the HD layer, the blue solid line represents the electron density n_{e2} of the NCD layer, and the red dashed line shows the proton density n_p of the NCD layer, respectively. In addition, the normalized longitudinal electric field E_x is also shown by the black dashed dotted line. Panels (a1) and (b1) are the results at $t = 1T_L$, panels (a2) and (b2) are at $t = 4T_L$, panels (a3) and (b3) are at $t = 9T_L$, panels (a4) and (b4) are at $t = 26T_L$.

Secondly, the evolution of the phase space distributions of the proton is shown in Fig. 3. Figures 3(a1)–3(a4) represent the results of the NCD target, and figures 3(b1)–3(b4) are those of the HD-NCD target. The four rows of Fig. 3 correspond to the snapshots at $t = 1T_L$, $t = 4T_L$, $t = 9T_L$, and $t = 26T_L$ respectively. In the NCD target, as shown in Fig. 3(a1), the p_x distribution of protons is still in the initial static state, which also proves that the protons remain at rest at the beginning of the interaction. Even when the laser penetrates through the NCD layer, as seen in Fig. 3(a2), the charge separation field

just causes a tiny fluctuation on the proton's p_x distribution. After the laser penetrates through the NCD layer, as seen in Fig. 3(a3), there occurs a broad phase space distribution of the proton. With the process of the acceleration, it can be seen that from Fig. 3(a4), the phase space distribution becomes broader and a long tail emerges in the pattern. However, for the HD-NCD target, an effective RPA process is presented in the right column of Fig. 3. At the beginning of the interaction, as seen in Fig. 3(b1), the protons of the NCD layer are also at rest since the laser pulse is just boring the HD layer due to the dense initial electron density. Then, it can be found that in Fig. 3(b2), the protons in the front of the NCD layer are rapidly accelerated due to the low penetrating velocity and the strong charge separation field, and there gradually emerges a twisting pattern. Then, most protons are caught in the acceleration field and a typical cocoon pattern of the RPA appears in Fig. 3(b3). Finally, the p_x distribution of the protons tend to be consistent, and there emerges a platform-like stable phase acceleration region, as shown in Fig. 3(b4).

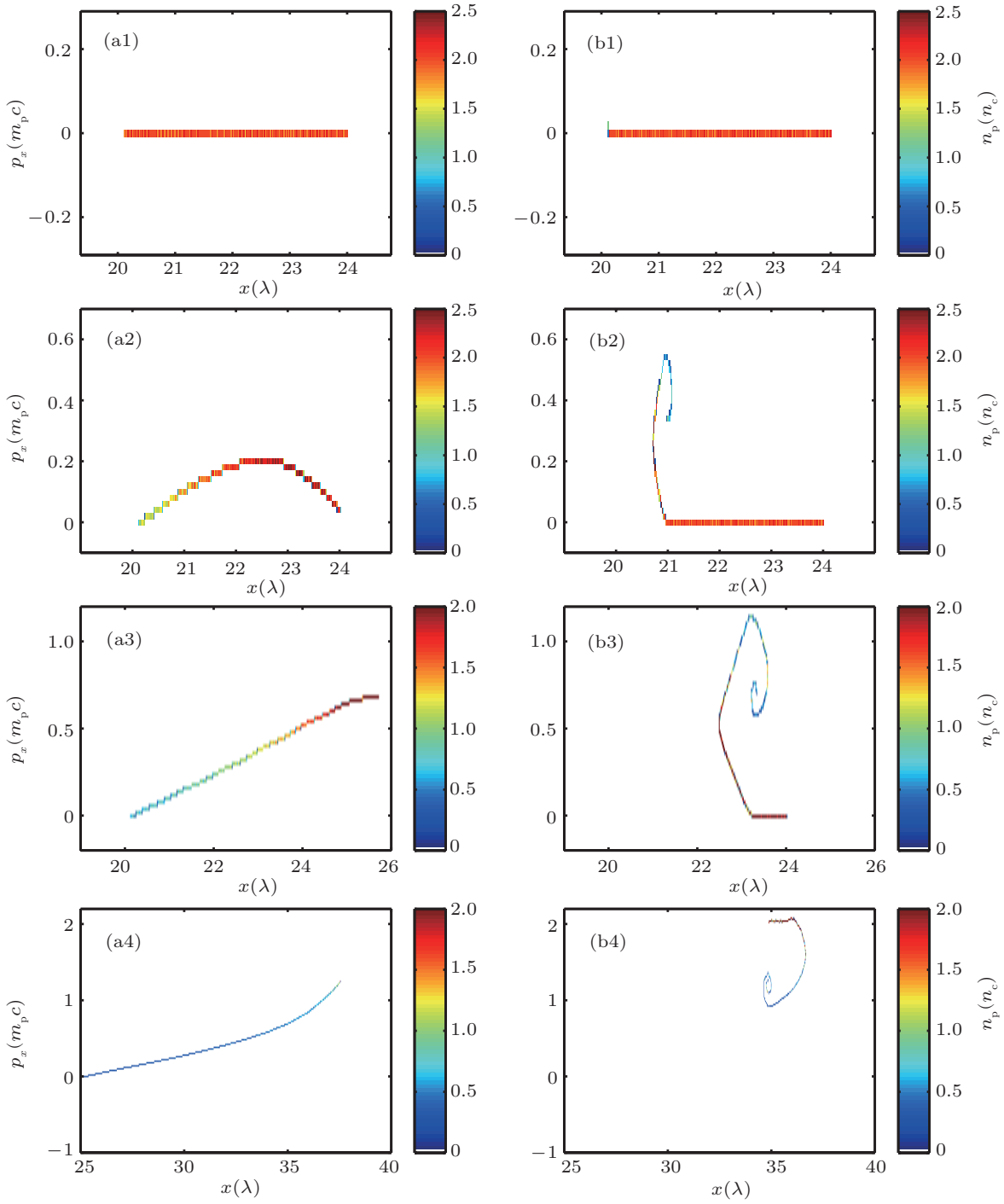


Fig. 3. (color online) The phase space distributions of the proton in the 1D simulations. The left column is the result of the NCD target and the right is of the HD-NCD target. Panels (a1) and (b1) are the results at $t = 1T_L$, panels (a2) and (b2) are at $t = 4T_L$, panels (a3) and (b3) are at $t = 9T_L$, panels (a4) and (b4) are at $t = 26T_L$.

It should be noticed that, in previous researches about the RPA,[19,20,22] in which the ultra-thin solid target is used, the accelerating field in the HB stage is generated by the charge separation of the ultra-thin solid target itself. When the intense laser pulse enters the foil target, the strong ponderomotive force pushes the electron forward and leaves the electron depletion layer behind. In the electron depletion layer, the protons under the linearly increased electrostatic field are accelerated and form the higher velocity flat-top in the phase space distribution. In the compressed electron layer, the protons under the linearly decreased electrostatic field are rapidly reflected to double electrostatic field velocity and form the lower velocity flat-top in the phase space distribution. Therefore, at the end of the HB stage, there appears the double flat-top structure in the phase space distribution of the proton.[22] However, in our scheme, the ultra high accelerating field in the HB stage is mainly generated by the charge separation in the HD layer of the target. When this strong electrostatic field along with the laser pulse enter the NCD layer, the proton in the NCD layer would be directly reflected by this fast moving electrostatic field and involved in the linearly decreased accelerating field, which leads to the single lower velocity flat-top in the phase space distribution of the proton. Therefore, in our scheme, the double-flat-top structure did not show up in the phase space distribution of the proton, as seen in Figs.3(b1)–3(b3). Since, the proton could be efficiently accelerated just in the linearly decreased accelerating field, the monoenergetic property of the accelerated proton beam can be effectively improved.

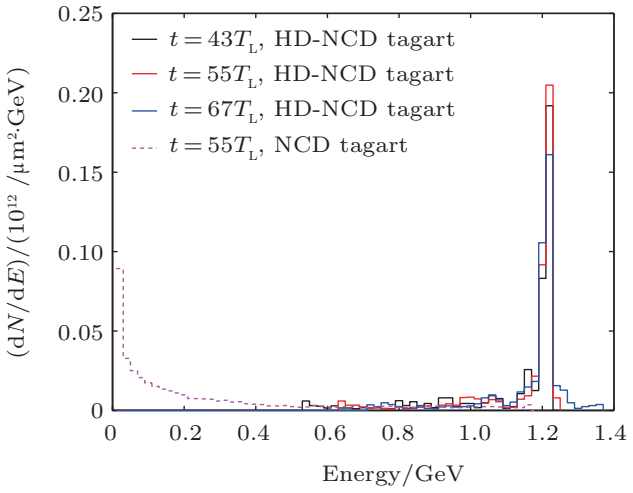


Fig. 4. (color online) The energy spectra of the proton in the 1D simulations. The dashed line is the result of the NCD target, and solid lines are the results of the HD-NCD target.

Finally, the energy spectra of the proton in the 1D simulations are presented in Fig. 4. For the NCD target, there is no energy peak in the energy spectrum. The majority of the protons are still in the low energy region, and the energy spectrum presents an exponential damping distribution. But for the HD-NCD target, there is an obvious single energy peak at $E = 1.2$ GeV through an effective RPA process, and the energy spread is only about 5%. In three specific moments, the energy spectra are nearly invariant, which means a more stable RPA of the proton is realized in the HD-NCD target.

3.2. Two-dimensional case

In the 1D PIC simulations, we have confirmed that a high quality proton beam can be generated through the stable RPA of the NCD target by the new scheme. In this part, the two-dimensional PIC simulations are performed to prove this new scheme. For the new scheme (HD-NCD target), the size of simulation box is 111 μm × 32 μm, which is composed of 11100×3200 cells along the x and y directions. The normalized amplitude of circularly polarized laser pulse

$$a = a_0 \exp\left[-(1/2)(y^{10}/r_0^{10})\right] \exp\left[-(1/2)((t-t_0)^2/T_0^2)\right]$$

with the waist radius $r_0 = 8$ μm. The transverse length of the target is 32 μm, which is corresponding to the region -16.0 μm $\leq y \leq 16.0$ μm. The other simulation parameters are the same as those of the one-dimensional case. We also performed a comparative simulation (NCD target), and there is also no HD layer in the target, i.e., a single NCD target is located in the region 20.1 μm $< x <$ 24.0 μm. The other simulation parameters are also the same as those of the HD-NCD target.

In the 2D case, figure 5 shows the snapshots of the spatial density distributions of the electron and the proton at $t = 1T_L$, $t = 4T_L$, $t = 9T_L$, and $t = 26T_L$, respectively. Figures 5(a1)–5(a4) represent the results of the NCD target, and figures 5(b1)–5(a4) represent the results of the HD-NCD target. By comparing Fig. 5 with Fig. 2, it is found that the acceleration characteristics are similar to those of the 1D simulations. In the NCD target, the electron layer is quickly pushed by the intense laser pulse without restriction, while the protons remain at rest, as shown in Figs. 5(a1) and 5(a2). After that, when the electron layer is completely ejected out of the target, the protons start to disperse by the inner repulsive force and the forward acceleration field, as seen in Figs. 5(a3) and 5(a4).

However, for the HD-NCD target, the intense laser pulse is effectively blocked by the HD layer and the penetrating velocity slows down sufficiently. Therefore, the protons can catch up with the electron layer, and a clear proton layer can be noticed distinctly, as shown from Figs. 5(b1)–5(b3). Finally, a typical radiation pressure acceleration structure emerges in Fig. 5(b4).

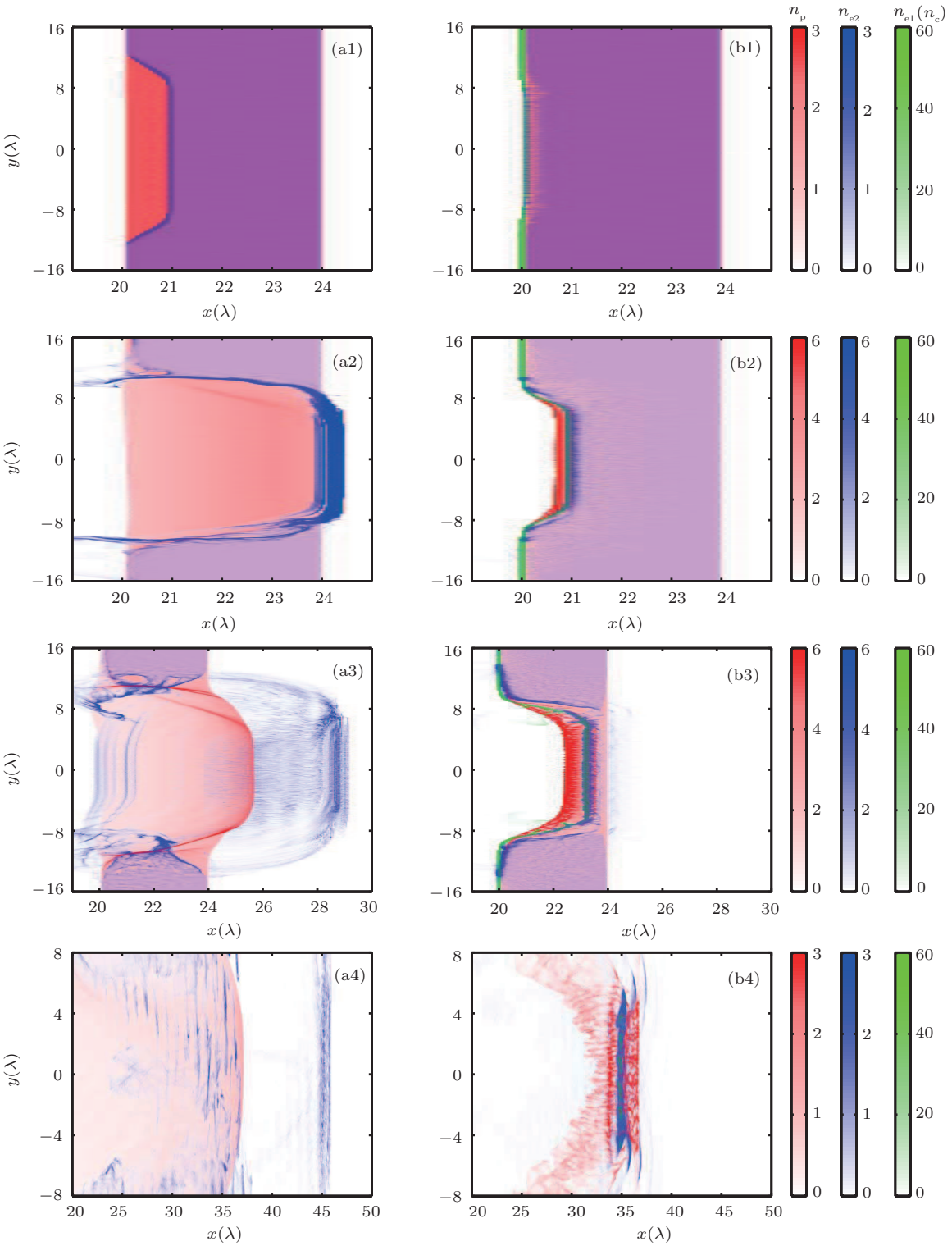


Fig. 5. (color online) The normalized density distributions of the electron and the proton in the 2D simulations. The left column is the result of the NCD target and the right column is of the HD-NCD target. Here, n_{e1} represents the electron density of the HD layer, n_{e2} and n_p denote the densities of the electron and the proton of the NCD layer, respectively. Panels (a1) and (b1) are the results at $t = 1T_L$, panels (a2) and (b2) are at $t = 4T_L$, panels (a3) and (b3) are at $t = 9T_L$, panels (a4) and (b4) are at $t = 26T_L$.

The evolution of the phase space distributions of the proton is presented in Fig. 6. By comparing Fig. 6 with Fig. 3, the phase space distributions of the proton in the 2D simulations agree well with those of the 1D case, except the pattern of Fig. 6(b4). Due to the high dimensional effects, some protons fall behind the major RPA structure and there appears an obvious long tail in the pattern. Those detached protons are separated from the main zone of the RPA field and gradually dumped in the acceleration, as shown in Figs. 6(b3) and 6(b4). Therefore, the main RPA structure and the detached proton part are gradually separated in the phase space distribution. Even so, the statistics suggests that about 70% protons are still accelerated to high energy region by the

RPA.

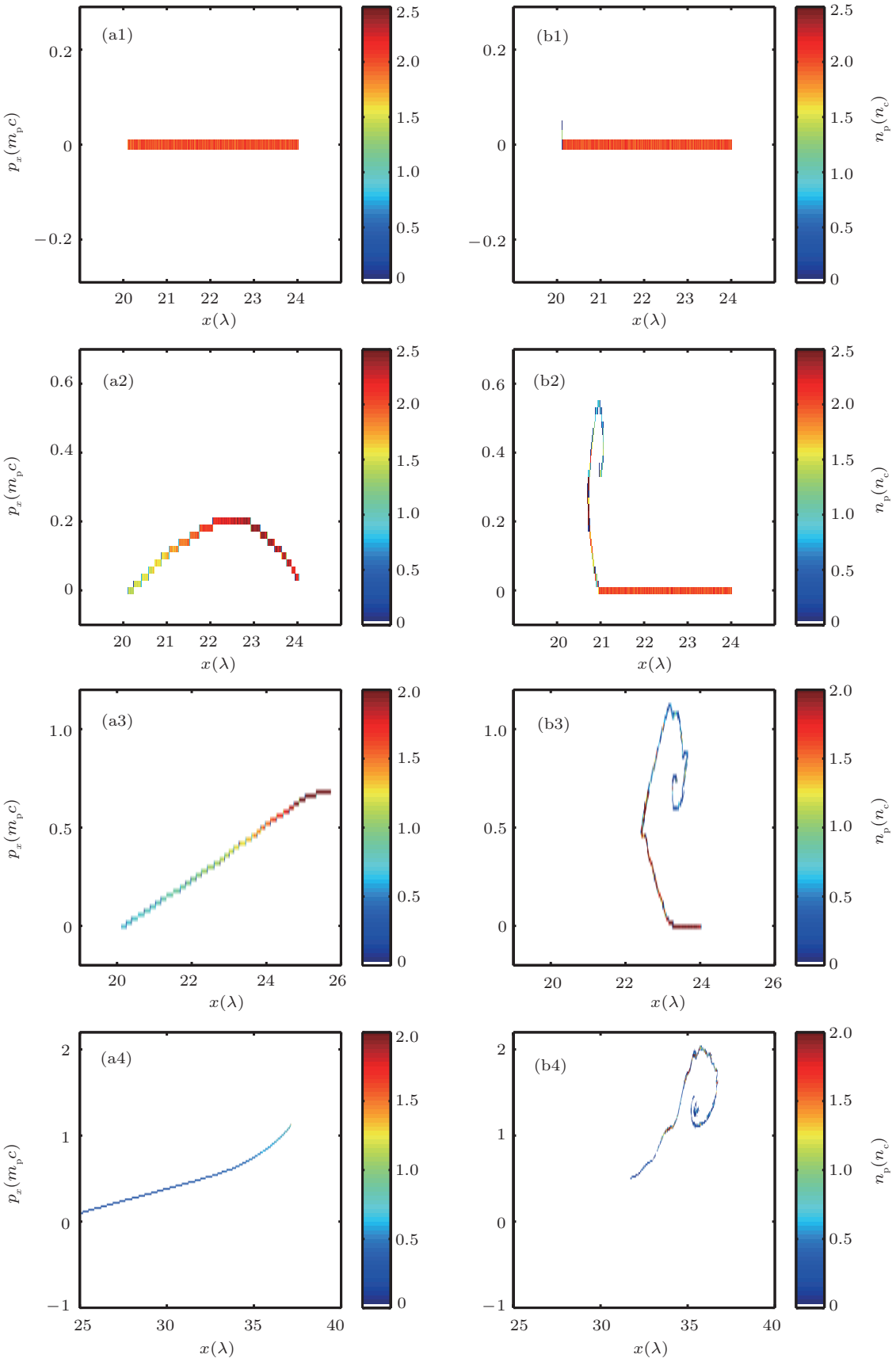


Fig. 6. (color online) The phase space distributions of the proton in the 2D simulations. The left column is the result of the NCD target and the right column is of the HD-NCD target. Here, we choose those protons that locate in the region $-0.02\ \mu\text{m} \leq y \leq 0.02\ \mu\text{m}$ as the object of statistics. Panels (a1) and (b1) are the results at $t = 1T_L$, panels (a2) and (b2) are at $t = 4T_L$, panels (a3) and (b3) are at $t = 9T_L$, panels (a4) and (b4) are at $t = 26T_L$.

The energy spectra and energy angular distributions of the proton in the 2D simulations are presented in Fig. 7. The left

column represents the NCD target, and the right column is of the HD-NCD target. For the NCD target, since it is unable to form an effective RPA structure in the acceleration, the protons are accelerated ineffectively and the energy spread of protons is nearly 100%, as seen in Fig. 7(a1). The energy distribution of protons presents an exponential damping spread and the majority of protons are in the low energy region, just like the 1D case. Furthermore, as shown in Fig. 7(a2), the proton that locates in the low energy region has a terrible angular distribution, which is from -20° to 20°. But for the HD-NCD target, as shown in Fig. 7(b1), the RPA of the NCD layer is realized and there appears an obvious energy peak at $E = 1.4$ GeV. Besides, as seen in Fig. 7(b2), most protons concentrate in the angle region between -5° to 5°, which shows a favorable collimation of the accelerated protons.

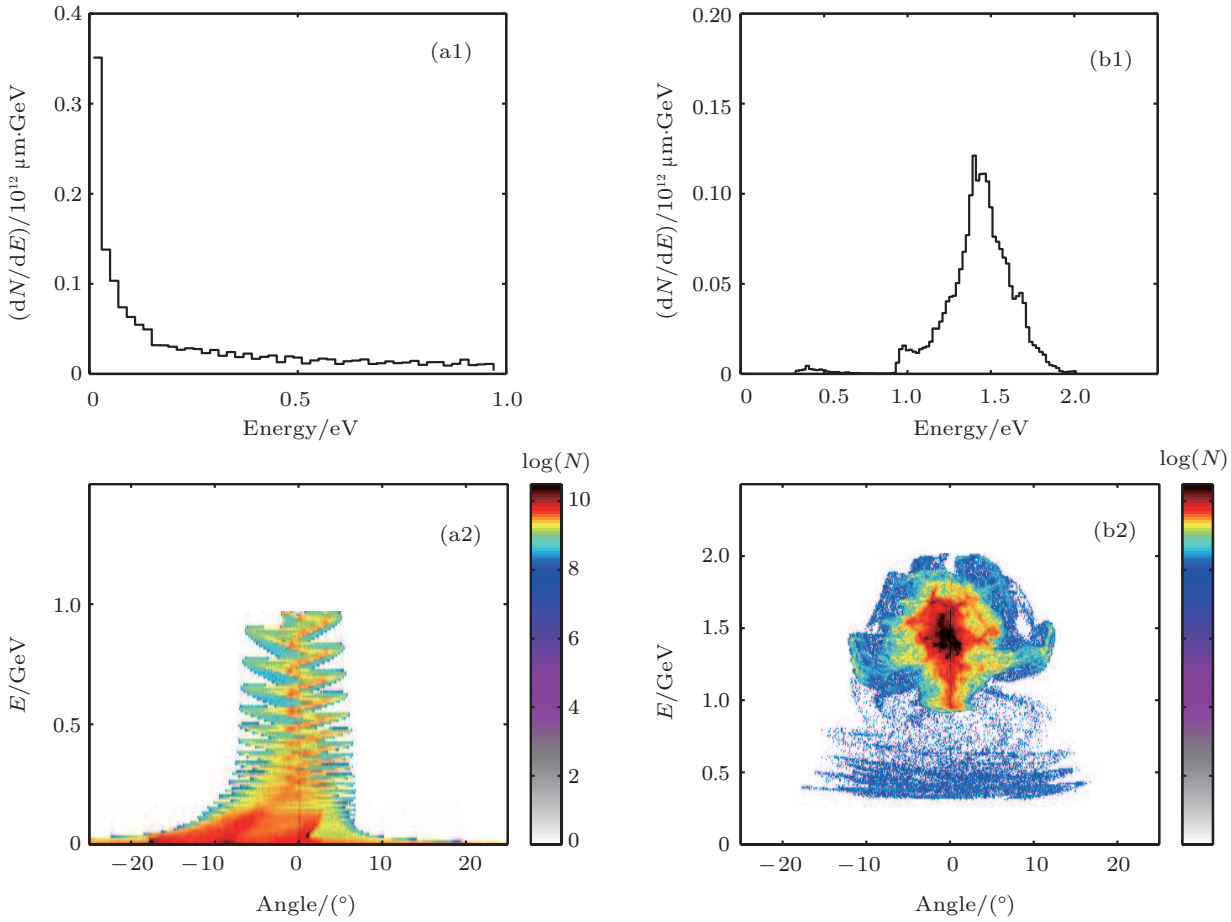


Fig. 7. (color online) The energy spectra and energy angle distributions of the proton in the 2D simulations. The left column is the result of the NCD target and the right column is of the HD-NCD target. Here, we choose those protons which locate in the region $-4\ \mu\text{m} \le y \le 4\ \mu\text{m}$ as the objects of statistics. For the new scheme, we just take the main RPA part into account. These results correspond to $t = 55T_\text{L}$, at the end of the acceleration.

4. Conclusion

In conclusion, for the sake of generating high quality ion beams through the stable RPA of the NCD target, we put forward a new type of target that an ultrathin HD layer is attached to the front surface of an NCD target. In the 1D PIC simulations, it is found that, when an intense laser pulse impinges on an NCD layer directly, the laser will propagate in the NCD layer due to the relativistic self-induced transparency. Therefore, the typical RPA structure cannot be formed and the protons are unable to be accelerated effectively. However, in the new scheme, by the block of the HD layer, the laser penetrating velocity is reduced effectively, and the proton can catch up with the fast-moving electron layer by the strong charge separation field. There emerges the HB process rather than the propagation in the NCD layer. As a result, a typical RPA structure that the compressed electron layer overlaps the proton layer as a whole can be formed. Eventually, the protons can be effectively accelerated to high energy in this RPA structure. By the use of carbon ions in the ultra-thin HD layer, a more efficient stable RPA is realized and a monoenergetic proton beam is obtained finally. Through this new scheme, a 1.2-GeV proton beam with an energy spread of only 5% is generated by using a circularly polarized laser pulse with the normalized laser amplitude $a = 120$. In the 2D PIC simulations, the accelerating characteristics of the proton are similar to those of the 1D simulations. Therefore, this new scheme is also applicative in a high dimensional situation. By varying the amplitude of the laser pulse, the thickness and the initial

electron density of the HD layer, it yields essentially similar results, which shows that our new scheme is robust. However, it should be noticed that, some other simulation parameters, including the parameters of the NCD layer, are not taken into account. The detailed simulation results on these parameter effects will be shown in our following paper. Compared with the traditional ultra-thin foil target, the most important meaning of the new scheme is that the thickness of the target in the new scheme is relatively larger, which means a preferable self-supporting property in reality. Therefore, this new type of target is an ideal substitution to the ultra-thin foil target in practical RPA experiments. Through this new scheme, a high quality ion beam can be obtained through the stable RPA of the NCD layer, which has many significant applications, i.e., tabletop accelerator, tumor therapy and inertial confinement fusion.

References

[1] Shearer J W, Garrison J, Wong J and Swain J E 1973 *Phys. Rev. A* **8** 1582

[2] Fourkal E, Shahine B, Ding M, Li J S, Tajima T and Ma C M 2002 *Med. Phys.* **29** 2788

[3] Roth M, Cowan T E, Key M H, Hatchett S P, Brown C, Fountain W, Johnson J, Pennington D M, Snavely R A, Wilks S C, Yasuike K, Ruhl H, Pegoraro F, Bulanov S V, Campbell E M, Perry M D and Powell H 2001 *Phys. Rev. Lett.* **86** 436

[4] Lan K, Li Y S, Wu C S, Gu P J, Pei W B, He X T, Li S W, Yi R Q, Jiang X H, He X A, Chui Y L, Liu Y G, Ding Y K and Liu S Y 2009 *Acta Phys. Sin.* **58** 3255 (in Chinese)

[5] Lu H Y, Wang C, Chen G L, Kim C J, Liu J S, Ni G Q, Li R X and Xu Z Z 2009 *Chin. Phys. B* **18** 537

[6] Forslund D W and Shonk C R 1970 *Phys. Rev. Lett.* **25** 1699

[7] Forslund D W and Freidberg J P 1971 *Phys. Rev. Lett.* **27** 1189

[8] Denavit J 1992 *Phys. Rev. Lett.* **69** 3052

[9] Silva L O, Marti M, Davies J R, Fonseca R A, Ren C, Tsung F S and Mori W B 2004 *Phys. Rev. Lett.* **92** 015002

[10] Maksimchuk A, Gu S, Flippo K, Umstadter D and Bychenkov V Y 2000 *Phys. Rev. Lett.* **84** 4108

[11] Snavely R A, Key M H, Hatchett S P, Cowan T E, Roth M, Phillips T W, Stoyer M A, Henry E A, Sangster T C, Singh M S, Wilks S C, MacKinnon A, Offenberger A, Pennington D M, Yasuike K , Langdon A B, Lasinski B F, Johnson J, Perry M D and Campbell E M 2000 *Phys. Rev. Lett.* **85** 2945

[12] Schreiber J, Bell F, Grüner F, Schramm U, Geissler M, Schnürer M, Ter-Avetisyan S, Hegelich B M, Cobble J, Brambrink E, Fuchs J, Audebert P and Habs D 2006 *Phys. Rev. Lett.* **97** 045005

[13] Askar'yan G A, Bulanov S V, Pagoraro F and Pukhov A M 1994 *JETP Lett.* **60** 251, ISSN: 0021-3640/94/040251-07

[14] Bulanov S V, Lontano M, Esirkepov T Z, Pegoraro F and Pukhov A M 1996 *Phys. Rev. Lett.* **76** 3562

[15] Mourou G, Chang Z, Maksimchuk A, Nees J, Bulanov S V, Bychenkov V Y, Esirkepov T Z, Naumova N M, Pegoraro F and Ruhl H 2002 *Plasma Phys. Rep.* **28** 12

[16] Fukuda Y, Faenov A Y, Tampo M, Pikuz T A, Nakamura T, Kando M, Hayashi Y, Yogo A, Sakaki H, Kameshima T, Pirozhkov A S, Ogura K, Mori M, Esirkepov T Z, Koga J, Boldarev A S, Gasilov V A, Magunov A I, Yamauchi T, Kodama R, Bolton P R, Kato Y, Tajima T, Daido H and Bulanov S V 2009 *Phys. Rev. Lett.* **103** 165003

[17] Esirkepov T, Borghesi M, Bulanov S V, Mourou G and Tajima T 2004 *Phys. Rev. Lett.* **92** 175003

[18] Shen B F and Xu Z Z 2001 *Phys. Rev. E* **64** 056406

[19] Macchi A, Cattani F, Liseykina T V and Cornolti F 2005 *Phys. Rev. Lett.* **94** 165003

[20] Zhang X M, Shen B F, Cang Y, Li X M, Jin Z Y and Wang F C 2007 *Phys. Lett. A* **369** 339

[21] Robinson A P L, Zepf M, Kar S, Evans R G and Bellei C 2008 *New J. Phys.* **10** 013021

[22] Yan X Q, Liu B C, He Z H, Sheng Z M, Guo Z Y, Lu Y R, Fang J X and Chen J E 2008 *Chin. Phys. Lett.* **25** 3330

[23] Henig A, Steinke S, Schnürer M, Sokollik T, Hörlein R, Kiefer D, Jung D, Schreiber J, Hegelich B M, Yan X Q, Meyer-ter-Vehn J, Tajima T, Nickles P V, Sandner W and Habs D 2009 *Phys. Rev. Lett.* **103** 245003

[24] Macchi A, Veghini S and Pegoraro F 2009 *Phys. Rev. Lett.* **103** 085003

[25] Jin Z Y, Shen B F, Zhang X M, Wang F C and Ji L L 2009 *Chin. Phys. B* **18** 5395

[26] Chen M, Pukhov A and Yu T P 2009 *Phys. Rev. Lett.* **103** 024801

[27] Qiao B, Zepf M, Borghesi M and Geissler M 2009 *Phys. Rev. Lett.* **102** 145002

[28] Robinson A P L, Gibbon P, Zepf M, Kar S, Evans R G and Bellei C 2009 *Plasma Phys. Control. Fusion* **51** 024004

[29] Robinson A P L, Kwon D H and Lancaster K 2009 *Plasma Phys. Control. Fusion* **51** 095006

[30] Yu T P, Pukhov A, Shvets G and Chen M 2010 *Phys. Rev. Lett.* **105** 065002

[31] Qiao B, Zepf M, Borghesi M, Dromey B, Geissler M, Karmakar A and Gibbon P 2010 *Phys. Rev. Lett.* **105** 155002

[32] Kar S, Kakolee K F, Qiao B, Macchi A, Cerchez M, Doria D, Geissler M, McKenna P, Neely D, Osterholz J, Prasad R, Quinn K, Ramakrishna B, Sarri G, Willi O, Yuan X Y, Zepf M and Borghesi M 2012 *Phys. Rev. Lett.* **109** 185006

[33] Macchi A, Borghesi M and Passoni M 2013 *Rev. Mod. Phys.* **85** 751

[34] Pae K H, Kim C M and Nam C H 2016 *Phys. Plasmas* **23** 033117

[35] Wang F C 2016 *Chin. Phys. B* **25** 054102

[36] Bin J H, Ma W J, Wang H Y, Streeter M J V, Kreuzer C, Kiefer D, Yeung M, Cousens S, Foster P S, Dromey B, Yan X Q, Ramis R, Meyer-ter-Vehn J, Zepf M and Schreiber J 2015 *Phys. Rev. Lett.* **115** 064801

[37] Wang J W, Yu W, Yu M Y, Xu H, Ju J J, Luan S X, Murakami M, Zepf M and Rykovanov S 2016 *Phys. Rev. Accel. Beams* **19** 021301

[38] Hu R H, Liu B, Lu H Y, Zhou M L, Lin C, Sheng Z M, Chen C E, He X T and Yan X Q 2015 *Sci. Rep.* **5** 15499

[39] Liu B, Hu R H, Wang H Y, Wu D, Liu J, Chen C E, Meyer-ter-Vehn J, Yan X Q and He X T 2015 *Phys. Plasmas* **22** 080704

[40] Shen B F, Zhang X M, Sheng Z M, Yu M Y and Cary J 2009 *Phys. Rev. ST Accel. Beams* **12** 121301

[41] Nieter C and Cary J R 2004 *J. Comput. Phys.* **196** 448

[42] Kaw P and Dawson J 1970 *Phys. Fluids* **13** 472

[43] Kruer W L 1988 *The Physics of Laser Plasma Interactions* (Boston: Addison-Wesley) p. 90